Rediniotis, O.K., and Lagoudas, D.C., "Shape Memory Alloy Actuator as Locomotor Muscles," rev. paper sub. to AIAA 3/21/01

SHAPE MEMORY ALLOY ACTUATORS AS LOCOMOTOR MUSCLES

Othon K. Rediniotis* and Dimitris C. Lagoudas‡

Aerospace Engineering Department

Texas A&M University, College Station, TX 77843-3141

Abstract

This work addresses the potential of Shape Memory Alloy (SMA) actuators as locomotor muscles in aquatic and avian biomimetic applications. Critical issues, such as actuator fatigue life, actuation bandwidth and energetics, are addressed. It is shown that the fatigue life of an actuator largely depends on the applied load and on the extent of the phase transformation. Our data indicates that, for partial thermally induced phase transformation, the fatigue life can be drastically increased with respect to full transformation cycles.

We counter the misconception that SMAs are not capable of high actuation bandwidths. It is shown that, actuation bandwidths of 20 Hz have been achieved for SMA wire actuation. Novel adaptive feedback controllers are also presented that can achieve excellent tracking at these actuation bandwidths. In order to achieve high SMA actuation frequencies, fast SMA cooling is required. An energetically efficient, active approach is to embed the SMAs inside closed-system channels, containing a temperature-controlled, circulating, cooling medium. This approach has several advantages. A cooling medium can be selected that has both low electrical conductivity and high thermal conductivity properties. The channels that embed the SMAs can be made out of a material, such as silicon rubber, that thermally and electrically insulates the cooling medium from the ambient environment, while its elastic properties can accommodate the SMA actuation displacements. An energetically important aspect of this approach is that only small, channel internal diameters are necessary to achieve large cooling rates. The SMA is surrounded by a small amount of coolant, therefore during SMA heating only small amounts of energy escapes to the coolant, especially if its circulation is temporarily halted.

---

* Associate Professor
‡ Ford Professor

Finally, results of on going research on an SMA actuated biomimetic autonomous underwater vehicle (AUV) are briefly presented.

Nomenclature

A	Austenite
A_F	Austenite finish temperature
A_S	Austenite start temperature
A_{0F}	Austenite finish temperature at zero stress
A_{0S}	Austenite finish temperature at zero stress
H	Hysteresis model
H^T_{max}	Maximum transformation strain
H^{-1}	Hysteresis model inverse
M	Martensite
M_F	Martensite finish temperature
M_S	Martensite start temperature
M_{0F}	Martensite finish temperature at zero stress
M_{0S}	Martensite finish temperature at zero stress
T_a	Annealing temperature
T_r	Reference temperature
$\overline{T}$	Estimated temperature
a_m	Gain to determine how fast $\overline{T}$ approaches T_r
b_m	Gain to determine how fast $\overline{T}$ approaches T_r
e_H	Error

i	Current signal
i_{max}	Pre-defined safety limit on current
r(t)	Reference displacement signal
u	Required heating
y	Actual displacement
$\hat{y}$	Estimate of the displacement output
α	Physical parameter based on heat convection from the sma wire
β	Physical parameter based on resistance of the sma wire
ε_{max}^{T}	Maximum transformation strain
ε_{min}^{T}	Minimum transformation strain
λ^0	Mean percentage of transformation strain
λ^a	Amplitude of transformation strain percentage
θ_{ij}	Hysteresis model parameters

Introduction

Bird flight has inspired and guided the design and development of aircraft since its inception. However, it is striking how primitive these man-made machines are compared to their natural counterparts in terms of efficiency, agility, coordination, autonomy and adaptability. In birds and insects, nature has evolved into a great synergy between muscles (actuators), wings (structure) and brain (control) that has not been approached in the most advanced aircraft and rotorcraft. In nature, every living organism that can generate lift does so through the flapping of wings. A significant advantage of flapping wing propulsion is that lift can be generated with little or no forward velocity and with small wing size.

In the area of underwater vehicle design, the development of small highly maneuverable vehicles is also presently of interest. Their design is based on the undulatory body motion, swimming techniques and anatomic structure of fish, primarily the highly controllable fins and the large aspect ratio lunate tail[1]. These pursuits in air and underwater vehicles triggered the emergence of the science of biomimetics, which is the study of natural systems in order to improve the design and functionality of synthetic systems[§]. The tailoring and implementation of the accumulated knowledge into biomimetic vehicles is obviously a task of multidisciplinary nature.

In biomimetics, the use of conventional systems of gears and servomotors to provide the actuation power leaves little interior room in the device for control systems and payload[**,††]. Especially in micro air vehicles, power density of the actuation system is a crucial design parameter. In actuator technology, active or "smart" materials have opened new horizons in terms of actuation simplicity, compactness, and miniaturization potential. With the current advances in Shape Memory Alloy (SMA) actuation technology, SMAs are probably the most suited actuators to a range of biomimetic applications[1].

As an illustration of the benefits of SMA actuation over other active materials such as piezoceramics and magnetostrictives, let us consider two biomimetic examples: first a flapping-wing micro air vehicle (FWμAV), with a wingspan of 6in to 12in with large wing-tip excursions. This means that during flapping, actuators with large actuation stroke/strain are preferable. Also, the small available on-board space dictates the use of high energy-density actuation systems.

[§] On-line Medical Dictionary, Academic Medical Publishing & CancerWEB, http: //www.graylab.ac.uk/cgi-bin/omd?biomimetics, 1997–98

[**] Barrett, D., "Design of the MIT Robo Tuna," MIT RoboTuna Home Page http://web.mit.edu/towtank/www/tuna/brad/design.html

[††] Kumph, J. M., "The Robot Pike Project," MIT Robot Pike Home Page, http://web.mit.edu/towtank/www/pike/stryrp.html

Piezoceramic and magnetostrictive materials have relatively low energy densities and high actuation frequencies, which are not required in this application. SMAs have energy densities much higher than piezoceramic materials. Furthermore, piezoceramic and magnetostrictive materials are only capable of producing small strains and displacements (small fractions of 1%) compared to those attained by SMA materials (as high as 8% for one-way trained and 4% for two-way trained SMAs)[2]. At first glance, the frequencies (on the order of 10 Hz) may seem too high for SMA actuation. As we will show later, this is a misconception. We will demonstrate that SMA actuation frequencies even higher than 10 Hz are possible and accurately controllable. Our previous work also indicates that thin SMA layers (~6μ thick) under partial transformation are capable of delivering frequencies of about 30 Hz at peak stress of 145 MPa[3]. Energy considerations for such an application are covered in a later section.

Consider a second example: a fish-like autonomous underwater vehicle (AUV) on the order of 1 m long. The vehicle is to be propelled by a caudal-fin equivalent system, with the ratio (caudal-fin trailing-edge excursion)/(vehicle length) maintained equal to an average value observed in the propulsion of its aquatic counterparts[4,5] (around 0.22). For the above data and for underwater vehicle speeds between 3 and 7 knots (1.5 m/sec to 3.5 m/sec), caudal-fin oscillation frequencies will range from 1.5 Hz to 5 Hz. The frequency bandwidth, combined with double-amplitude trailing-edge excursions on the order of 0.25 m, makes SMA-based actuation ideal for the particular application. A six-segment biomimetic hydrofoil[1] has been developed and is currently under testing and modifications to evaluate the use of SMAs to power such an AUV. Results are discussed in a later section.

The small sizes and high force densities of SMAs (compared to conventional actuators) result in availability of much larger percentage of vehicle internal volume. This greater internal

volume allows for a larger payload for comparably sized vehicles. Additional SMA advantages include: (a) Simplicity of actuation mechanism. SMAs can be all-electric devices and can be used as "Direct Drive Linear Actuators" requiring little or no additional gear reduction or motion amplification hardware. These merits permit the realization of small or even miniature actuation systems in order to overcome space limitations. (b) Silent actuation. Since no acoustic signature is associated with such a propulsion system, acoustic detectability will be reduced. (c) Low driving voltages, when powered electrically. Nitinol (NiTi) SMAs can be actuated with very low voltages (10 to 20 V), thus requiring very simple power supply hardware. In contrast, piezoceramic materials typically require voltages on the order of 100 V for their actuation. However, for SMAs large currents may be required for resistive heating, depending on SMA actuator dimensions, leading to heavy power supply hardware. (d) SMAs are heat engines, which means that they do not necessarily need to be powered electrically. The electrical power required to actuate SMAs with loads, frequencies and fatigue life, practical for dynamic applications, demand the use of relatively heavy power supplies/batteries, which in turn results in high system weights and poor energy densities. But as heat engines, they can utilize on-board parasitic heat, if available, to produce useful mechanical work. If parasitic heat is not available, they can readily use the chemical energy of fuels, which have outstanding energy densities (order of 13,000 Wh/Kg or 46,800 KJ/Kg) compared to compact batteries (125 – 300)Wh/kg or (450-1080) KJ/Kg. As an example, schematics with heating and cooling cycles for such a configuration are shown in figure 13 and presented in a later section.

SMA actuation is not free of drawbacks, however. Some of them, such as actuation loss and fatigue over repetitive cyclic loading, are in the frontier of SMA research. Many researchers have investigated the effect of both mechanical and thermal cyclic loading on the

thermomechanical response of NiTi [6-11]. However, these tests were primarily concerned with the development and stability of two-way strain, the evolution of plastic strain, or hardening in the stress-strain response.

Extension of the cyclic loading path until specimen failure occurs has been studied by a limited number of researchers, with the primary emphasis on mechanical transformation fatigue (i.e., a stress-induced phase transformation). Melton and Mercier[12] gave the earliest detailed report on fatigue properties for NiTi specimens. Constant stress amplitude fatigue results (S-N curves) showed that fatigue limits reached 10^7 cycles for stress levels which did not induce a phase transformation. The fatigue life for stress amplitudes that induced phase transformations (i.e., mechanical transformation fatigue) was reduced to approximately 10^3 to 10^4 cycles. Constant strain amplitude fatigue results that included a phase transformation showed that low cycle fatigue obeyed the Coffin-Manson law relating plastic strain and cycles to failure[13].

Miyazaki[14,15] and Tobushi et al.[16,17] have performed some of the most recent work on stress-induced transformation fatigue. Miyazaki performed an isothermal cyclic tensile loading at constant stress amplitude, similar to Melton and Mercier[12], for different test temperatures. Due to the lower percentage of martensitic transformation associated with elevated test temperatures, a higher fatigue life was identified, approaching 10^6 cycles. Study of the thermal transformation fatigue of NiTi SMA was performed by McNichols et al[18]. Results from this study showed a thermal transformation fatigue life between 10^4 and 10^5 cycles for constant strain amplitude levels between 4.4% and 8.3%. It appears that the thermally induced phase transformation fatigue of SMAs has not been studied systematically and the effect of the magnitude of transformation strain on the fatigue life of SMAs needs to be explicitly examined.

The remaining sections of this paper start with an overview of SMA actuators, followed by sections on thermomechanical transformation fatigue, adaptive control and energy considerations for SMA actuators. In the end, actual implementation of SMA actuators for an AUV are briefly reviewed and are followed by conclusions and acknowledgements.

Brief Overview of SMA Actuators

Our research has focused on Nitinol, which is a nickel-titanium based SMA alloy. In fact, Nitinol was the first shape memory alloy to be discovered. The name comes from the two element symbols, Ni and Ti, and the abbreviation of the lab where the alloy was discovered, the Naval Ordinance Laboratories (NOL)[19] . Shape memory properties of nitinol become evident once a specimen has been properly annealed.

The shape memory effect comes from the differences in the crystalline structure between the martensitic and austenitic states. Figure 1 shows the difference between the two crystal structures. Properties of the SMA vary depending on the amount of martensite/austenite present. The percentages of each state depend on the stress and temperature of the specimen[‡‡] Figure 2 shows a qualitative plot of the stress-temperature combinations at which each state exists. To the left of martensite finish M_F, only martensite is present. To the right of austenite finish A_F, only austenite is present. In between M_F and A_F, there is a combination of martensite and austenite. When the wire is deformed in the martensitic state and the temperature is raised above austenite start A_S, the wire will begin to return to its original shape and will be at the original shape when the temperature is above A_F. The above process is called one-way training[20]. If this process is repeated (that is, if a specimen is deformed in martensite, heated to austenite, and cooled to

‡‡ "An Introduction to Shape Memory Alloys," SMART-Homepage, http://smart.tamu. edu/pageIntro.htm

martensite), the wire will develop what is called two-way training[20]. It will expand by the trained amount when the temperature drops below M_F without a load on the wire.

A qualitative schematic of the SMA phase transformation diagram is shown in Figure 3 to clarify the actuator functions. The phase change in Nitinol is accompanied by a significant exchange of heat with the surroundings. The time rate of the transformation is controlled solely by the time rate of the heat transfer. Typically, SMA heating, which triggers the martensite-to-austenite (M-to-A) phase change, is achieved electrically (by resistive heating). The heating rate, and thus the transformation rate, can be controlled by regulating the applied voltage and thus the electrical current. To trigger the reverse transformation (A to M), heat removal from the SMA is necessary. Conventional heat-removal mechanisms are inherently slower than electrical heat-addition and usually rely on forced convection. Therefore, in a complete heating-cooling cycle (transformation/actuation, M to A and then A to M), the cooling process usually limits the speed of the cycle (i.e., the maximum attainable frequency response). An effort has been made to address this problem in a later section.

Another important consideration is that unless SMA actuators are properly employed, plastic strains may develop and the required force or displacement may not be attained on actuation. This variation in thermomechanical response requires further understanding of its influence for successful implementation of SMA actuators. To develop a better understanding of the thermomechanical response a discussion on the thermomechanical fatigue of the NiTi SMA actuator is provided in the following section.

Thermomechanical Transformation Fatigue of SMA Actuators

In many applications of SMA actuators, the Shape Memory Effect (SME) is used many times by heating and cooling and/or loading and unloading. A test frame and experimental setup developed in earlier work[21] was used to determine the thermal transformation fatigue life of SMA wires. The loading paths shown in Figure 4 represent the various ways in which SMAs were loaded. Loading Paths 1 and 3 do not contain a phase transformation of any kind. Therefore, in terms of transformation fatigue characterization, it is assumed that these tests would result in a response typical of mechanical fatigue seen in common engineering materials. Loading Path 2 shows a stress-induced martensitic phase transformation and represents the mechanical transformation fatigue loading path studied by previous researchers[12,14]. Loading Paths 4 and 5 show a thermally induced phase transformation and best describe the conditions seen by SMA actuators.

Two important experimental findings have been revealed that are related to the fatigue response of SMA wire actuators. The first finding relates the transformation fatigue life of NiTiCu to the heat treatment temperature, which was studied by Miller and Lagoudas[22] and Lagoudas et al.[23]. It is found that M_S and A_S temperatures increase slightly as annealing temperature (T_a) increases when the wire is annealed below 400°C, while a drastic increase is found in the interval of 450°C–550°C. Figure 5 shows a typical curve of different strains developed in the cycling process. A common feature in all samples is the large plastic strain developed during the first 300–500 cycles, which saturated to a nearly constant value during higher cycles.

The second experimental finding is the effect of stress level on the fatigue life of SMA wires. Cyclic thermal transformations were performed on NiTiCu wires that had a nominal

diameter of 0.6 mm and an initial cold work of 30%. Prior to testing, the wires were heat-treated at 600°C for 30 minutes and at 550°C for 15 minutes. Results for thermal transformation fatigue tests under a complete phase transformation and varying levels of constant applied stress are shown in Figure 6. The results show that, for higher stress levels, fewer cycles were needed to cause the specimen to fail and subsequently as the stress level decreases, the number of cycles to failure increases substantially.

Besides these fully transformed (major loop) fatigue tests, partially transformed (minor loop) fatigue tests were performed by Lagoudas et al.[23]. Partial transformation cycles were created by an incomplete martensitic transformation. The percentage of the transformation was controlled by choosing different levels of the mean percentage of transformation strain λ^0 and the amplitude of transformation strain percentage λ^a (shown in Figure 7), which were percentages of the complete transformation. Tests were performed for partial thermal transformation fatigue under a constant applied stress of 78.8 MPa. Prior to testing, the wires were annealed at 600°C for 30 minutes. A summary of the results is shown in Figure 8. Error estimates for strain values for both Figures 5 and 8 is in the order of ±0.075%.

Results so far indicate that, for partial thermally induced phase transformation, the fatigue life can be drastically increased with respect to full transformation cycles. Hence the idea of using multiple actuators with partial transformations may provide better actuation response. The following section discusses the developed control scheme for SMA actuators along with a method of achieving higher cooling rates.

Adaptive Control of SMA Actuator Wires

Exposure of the SMA actuators to the ambient medium has adverse effects the SMA control. In warm environments, the SMA cooling rate may not be sufficient, and in cold environments, the energy expended to heat up the SMAs to austenite may be too large depending on actuator applications. In order to achieve SMA actuation frequencies high enough to generate propulsive and maneuvering forces for FWμAVs and AUVs, forced convection cooling of the SMAs must be used. It was therefore decided to thermally insulate the SMA actuators from the ambient environment and embed them inside closed-system channels containing a temperature-controlled cooling medium.

In situations where electrical heating for M to A transformation and forced cooling for A to M transformation is utilized for actuation, one difficulty imposed by forced convection is that temperature measurements of the SMA cannot be achieved via thermocouples. A thermocouple is usually attached to the SMA wire/strip with a small "ball" of thermal paste, that is thermally, but not electrically, conductive. However, due to the strong heat transfer caused by active convection of the cooling medium, the thermal paste dissipates the heat, from the wire to the ambient medium, much faster compared to a pure conduction environment. This causes the resulting temperature measurement to not be an exact representation of the SMA temperature.

We have pursued actuation control schemes that rely only on actuator displacement feedback and do not require temperature feedback. The control approach in this work implements an adaptive hysteresis model for feedback compensation for control of SMA wire actuators[24,25] . In feedback compensation, the tracking error was not directly used in the control law. Rather, it was used to update (identify on-line) the hysteresis model (H) to account for discrepancies between the model and the actual input-output relationship. The inverse maps a

desired reference trajectory into a temperature signal. When temperature can be measured, an adaptive thermal model then commands a current to control the temperature of the SMA to track the desired temperature. For cases where temperature measurements are unavailable, integration of a simplified thermal model (based only on rough estimates of the thermal parameters) was used in place of actual temperature measurements.

The control algorithm used for a single-wire test setup can best be described by referring to the schematic in Figure. 9. The reference displacement signal *r(t)* was mapped into a reference temperature T_r via the hysteresis model inverse H^1. u is the heating required to force $\bar{T}$ to track T_r . The current signal i is the input to the SMA wire. The current was also limited by strict bounds on u given by $u \in [0, i_{\max}^2]$, where $i_{\max}$ was a pre-defined safety limit on the current. The lower limit on u essentially meant that the fastest cooling that could be achieved was when the current to the SMA wire was turned off. Gains that determined how fast $\bar{T}$ would approach T_r were $a_m = b_m$. α and β, and were physical parameters based on the convection and the resistance of the wire, respectively.

To adaptively update the hysteresis model to represent the y-versus-$\bar{T}$ relationship, the estimate $\hat{y}$ of the displacement output was generated from $H(\bar{T})$. The estimation error was calculated using the error between $\hat{y}$ and the actual displacement y. The hysteresis model parameters θ_{ij} were updated using the gradient adaptive law from Section 3.1.2 of Reference 24, in turn updating the inverse model.

In this control method, the thermal parameters remain constant. Although it may be possible to adaptively update the thermal parameters to represent the heating and convection more accurately for a time-varying cooling environment, for the results presented, the burden of accounting for these variations lies solely with the adaptive hysteresis model. Reasonable

estimates of the thermal parameters served to ensure that $\bar{T}$ remained in the defined input region of the hysteresis model[24].

Figure 10 is a schematic of the experimental setup[1] used to test the SMA control theory. The C shape of the test stand provided support for the wire while allowing easy access to the wire. The wire was embedded in a cooling channel. The SMA wire was connected to power leads by brass connectors, one on each end. The free end (top) of the wire was attached to the lever arm by a kevlar string. A spring attached to the opposite end of the lever arm both held the SMA wire in tension and provided a restoring force for the SMA. The spring was used instead of a constant weight (mass) as inertial forces created by a dead mass at higher frequencies caused the SMA wire to bounce, resulting in compressive forces on the SMA wire. Displacements were then measured using a Celesco string-potentiometer. The resolution of the string-potentiometer, in conjunction with a 16-bit data acquisition board (National Instruments AT-MIO-16XE-50), was 0.0008 inches. The total worst-case uncertainty was 0.011 inches in absolute position. The average wire used in the test frame was 12 inches long, so at 2% strain, and with a lever motion amplification of 4 to 1, this resulted in a displacement uncertainty of 1.15%.

On application of our adaptive control scheme to water-cooled SMA actuators for this experimental setup, good tracking for actuation frequencies as high as 20Hz was achieved. Figure 11 presents the control results for the case of using cool air as the convection medium. As shown, the tracking was very good, but due to the limited convection rates of air, only low actuation frequencies could be achieved. Figure 12 presents the tracking control results for the case of using water as the convection medium. Tracking was very good, and actuation frequencies as high as 20Hz were achieved.

Energy Considerations for SMA Actuators

It should be kept in mind here that SMAs are actuated by heat, which means that one does not necessarily have to use electricity to actuate them. One would rather use the chemical energy of fuels. We are in the process of developing small combustors along with active transfer of the heat to and from the SMA. Figure 13 shows a compact SMA actuator system, which comprises of mini pumps, a combustor, the SMA actuator, a heat exchanger and fuel as the energy source. Propane or Gasoline is used as the fuel since their energy densities are on the order of (50,000KJ/Kg), which is much higher than energy densities of batteries or fuelcells. Ethylene Glycol is considered as the heating fluid due to its high boiling point. It is heated in a combustor, which acts like a high efficiency boiler. The hot Ethylene Glycol heats the SMA actuator convectively above Austenite finish temperature causing strain recovery and hence actuation. Ethylene Glycol is circulated in the heating circuit through a pump. Another pump is used to circulate the coolant in the cooling circuit for cooling the SMA down to the Martensite finish temperature. A small battery operates these two pumps. The coolant is also circulated through a heat exchanger to dissipate heat removed from the SMA actuator.

Let us consider the following example: A typical, generic fuel has an energy density (enthalpy) of 13,000 Wh/Kg (48,800 KJ/Kg). The full transformation latent heat per unit volume for a typical SMA is 0.10 J/mm^3. For a flapping wing μAV with a wingspan on the order of 0.3 m, approximately 300 mm (length) of NiTi wire with a diameter of 0.6 mm (0.023") (keeping in mind that a NiTi wire of that diameter can pull, when actuated, as much as 70 N or 15.7 lbf) is considered. For an average flapping frequency of 20 Hz, the amount of wire mentioned above (a total of 85 mm^3) would need a total of 170 J/s. Assuming full transformation per cycle and a combustion efficiency of approximately 85% (typical of high efficiency boilers) a gram of fuel

will be sufficient to maintain the vehicle in cruise for about 4 min. The same calculations for a wingspan of 0.15 m (6") yields a flying time of approximately 8 min/g of fuel. Note that this analysis is based on full transformations. Partial transformation with multiple thin SMA actuators, would give higher frequency response[3] and less fuel consumption per SMA layer, yielding greater flying time for a given wing span.

To get an idea about work done per unit muscle mass (J/Kg), we compare typical work done by an SMA muscle to that done by a typical dragonfly and a hummingbird wing muscle as shown in Table 1. The reason for choosing hummingbirds and dragonflies is in accordance with the general understanding that development of a FWμAV based on biomimetics require study of flight mechanisms and characteristics as found in hummingbirds, dragonflies, and other flapping-wing insects. Based on conservative estimates, the work done by a typical SMA actuator per unit mass surpasses the estimates for hummingbirds and dragonflies. Of course, this fact alone does not justify usage of SMA for FWμAV. However, this combined with recent developments, like smaller system weight/size, high actuation frequencies, high energy densities, active heating/cooling and relatively high fatigue life, provides enough incentive for SMA actuators to be considered as an alternative.

Table 1. Work done per muscle mass

Muscle Type	Work done per muscle mass (J/kg)
Dragon Fly (S.sanguineum)[26]	4
Hummingbird[27]	2–7.41
SMA	1000

SMA Actuators as Locomotor Muscles for a Biomimetic Hydrofoil

The profile shape of the six-segment biomimetic hydrofoil[1] was based on an NACA 0009 airfoil section with a 30-inch (76.2-cm) chord and minor modifications in the aft portion of the profile. There are three main components to the biomimetic hydrofoil: a) the aluminum backbone and rib structure, b) the SMA muscles, and c) the scales or skin.

The ribs are seven 0.25-inch-thick (0.64-cm) aluminum plates. The seven ribs are connected with six sets of hinge pairs (vertebrae). The vertebrae are machined aluminum, with bearings at the pivot points to ensure smooth motion between the ribs. Mounted on each vertebra of each pair is a position encoder. The encoder gives the relative angle between adjacent ribs.

The SMA muscle has two parts that pull in opposing directions. The opposing force is provided by two springs. The SMA wires run parallel to the segments, as shown in Fig. 14. This orientation allows the wires to be longer, and with a pulley system a larger angular displacement of the vertebrae is achieved.

The skin is the interface between the vehicle and the ambient fluid and allows the hydrofoil to efficiently transfer energy to the fluid, thus generating thrust. The skin is set up as six overlapping scales on each side, with nose and tail sections added at the leading and the trailing edge respectively. Fig 15 shows the fully assembled hydrofoil.

In-air actuation tests were performed to track various types of reference signals. Water tunnel actuation was performed to track several types of reference signals and to measure the thrust generated by the resulting hydrofoil shapes. Sinusoidal deflection patterns were also tested for thrust producing capabilities. Fig. 1 shows a picture from one such actuation cycle.

Conclusions

Controllable actuation of SMAs up to 20Hz has been demonstrated. Increasing actuation bandwidth would require using active temperature controlled cooling medium. We are in the process of implementing SMA actuators that utilize partial transformation and active cooling and are capable of actuation bandwidths of 50 to 100 Hz.

It has been shown that fatigue life of SMAs depends upon dislocation density, applied load and the extent of phase transformation. Fatigue life increases under reduced load and partial phase transformation. Areas such as low energy efficiency and relatively high current requirements for SMA actuators, if electric SMA heating is utilized, need to be addressed.

Small fuel combustors coupled with active transfer of heat to and from the SMA are being researched as high energy-density sources for SMAs. An effort has been made to provide a general proof of concept of using SMAs as locomotor muscles for FWμAV and AUV. Actual implementation of SMAs as locomotor muscles for a biomimetic hydrofoil has been discussed and acts as a stepping stone towards further development and understanding of SMA actuated FWμAV and AUVs.

Acknowledgement

The authors wish to acknowledge the financial support for the research on the Biomimetic Hydrofoil by the Office of Naval Research, Contract No. N00014-97-1-0840 and Aeroprobe Corporation, Project No. 96-386. The sponsorship by the Texas Higher Education Coordination Board, TD&T Grant No. 000512-0278-1999, is also gratefully acknowledged. The authors would also like to acknowledge the help of Mughees Khan in the preparation of the manuscript.

References

1. Rediniotis, O. K., Lagoudas, D. C., and Wilson, L. N., "Development of a Shape Memory Alloy Actuated Biomimetic Hydrofoil," AIAA Paper No. 2000-521, 38th Aerospace Science Meeting and Exhibit, Reno, Nevada, Jan. 2000.

2. Tobushi, H., Ohashi, Y., Saida, H., Hori, T., and Shirai, S., *JSME Int. Journal*, vol. I, 84, 1992.

3. Lagoudas, D. C. and Bhattacharyya, A., "Modeling of Thin Layer Extensional Thermoelectric SMA Actuators", *International Journal of Solids and Structures*, Vol. 35, No. 3–4, 1998, pp. 331–362.

4. Kudva, J., Jardine, P., Martin, C., and Appa, K., "Overview of the ARPA/WL 'Smart Structures and Materials Development – Smart Wing' Contract," 3rd SPIE Symposium on Smart Structures and Materials, San Diego CA, 1996.

5. Gilbert, W. W., "Mission Adaptive Wing System for Tactical Aircraft," Journal of Aircraft, Vol. 18, No. 7, 1981, pp. 597-602.

6. Hebda, D. and White, S. R., "Effect of Training Conditions and Extended Thermal Cycling on Nitinol Two-Way Shape Memory Behavior", *Smart Materials and Structures*, Vol. 4, 1995, pp. 298–304.

7. Lim, T. J. and McDowell, D. L., "Degradation of an NiTi Alloy During Cyclic Loading," *Proceedings of the 1994 North American Conference on Smart Structures and Materials*, SPIE, Orlando, Florida, 1994, pp. 153–165.

8. Miyazaki, S., Imai, T., Igo, Y., and Otsuka, K., "Effect of Cyclic Deformation on the Pseudoelasticity Characteristics of Ti-Ni Alloys," *Metallurgical Transactions A*, Vol. 17, 1986, pp. 115–120.

9. Tanaka, K., Nishimura, F., Hayashi, T., Tobushi, H., and Lexcellent, C., "Phenomenological Analysis on Subloops and Cyclic Behavior in Shape-Memory Alloys Under Mechanical and or Thermal Loads," *Mechanics of Materials*, Vol. 19, 1995, pp. 281–292.

10. Lagoudas, D. C. and Bo, Z., "Thermomechanical Modeling of Poly-crystalline SMAs Under Cyclic Loading, Part II: Material Characterization and Experimental Results for a Stable Transformation Cycle," *International Journal of Engineering Science*, Vol. 37, 1999, pp. 1141–1173.

11. McCormick, P. G. and Liu, Y., "Thermodynamic Analysis of the Martensitic Transformation in NiTi. 1. Effect of Heat-Treatment on Transformation Behavior," *Acta Metallurgica el Materialia*, Vol. 42, No. 7, 1994, pp. 2401–2406.

12. Melton, K. N. and Mercier, O., "Fatigue of NiTi Thermoelastic Martensites," *Acta Metallurgica*, Vol. 27, 1979, pp. 137–144.

13. Suresh, S., *Fatigue of Metals,* Cambridge University Press, Cambridge, 1991.

14. Miyazaki, S., *Engineering Aspects of Shape Memory Alloys*, edited by T. W. Duerig, K. N. Melton, D. Stockel, and C. M. Wayman, Butterworth-Heinemann, London, 1990, p. 394.

15. Miyazaki, S., Mizukoshi, K., Ueki, T., Sakuma, T., and Liu, Y., "Fatigue Life of Ti-50 at. % Ni and Ti-40Ni-10Cu (at. %) Shape Memory Alloy Wires," *Materials Science and Engineering A*, Vol. 273–275, 1999, pp.658–663.

16. Tobushi, H., Hachisuka, T., Yamada, S., and Lin, P.-H., "Rotating-Bending Fatigue of a TiNi Shape-Memory Alloy Wire," *Mechanics of Materials*, Vol. 26, 1997, pp. 35–42.

17 Tobushi, H., Hachisuka, T., Hashimoto, T., and Yamada, S., "Cyclic Deformation and Fatigue of a TiNi Shape Memory Alloy Wire Subjected to Rotating Bending," *Journal of Engineering Materials and Technology*, Vol. 120, 1998, pp. 64–70.

18. McNichols, J. L. and Brooks, P. C., "NiTi Fatigue Behavior," *Journal of Applied Physics*, Vol. 52, 1981, pp. 7442–7444.

19.Buehler, W.J., Wiley, R.C., "Nickel-based alloys," US Patent 3,174,851, 1965.

20. Wayman, C. M., *Phase Transformations, Nondiffusive*, BV: Elsevier, 1983.

21. Lagoudas, D. C. and Miller, D. A., "Experiments of Thermomechanical Fatigue of SMAs," *Proceedings of the 1999 Conference on Smart Structures and Materials*, SPIE, 1999, pp. 275–282.

22. Miller, D. A. and Lagoudas, D. C., "Influence of Cold Work and Heat on the Shape Memory Effect and Plastic Strain Development of NiTi Wire Actuators" submitted to *Materials Science and Engineering A*, 2000.

23. Lagoudas, D. C., Miller, D. A., Rong, L. and Li, C., "Thermomechanical Transformation Fatigue of SMA Actuators," submitted to *Proceedings of the 2000 Conference on Smart Structures and Materials*, SPIE, 2000.

24. Webb, G., Wilson, L., Rediniotis, O., Lagoudas, D., "Adaptive Control for Shape Memory Alloys Wires in Under Water Applications," *AIAA Journal*, Vol. 37, No. 11, 1999.

25. Webb, G. V., "Adaptive Identification and Compensation for a Class of Hysteresis Operators," Ph.D. Dissertation, Department of Aerospace Engineering, Texas A&M University, College Station, Texas, 1998.

26. Wakeling, J. M. and Ellington, C. P., "Dragon Fly Flight: III. Lift and Power Requirements," *Journal of Experimental Biology*, Vol. 200, 1997, pp. 583–600.

27. Chai, P., "Hummingbird Hovering Energetics During Moult of Primary Flight Feathers," *Journal of Experimental Biology*, Vol. 200, 1997, pp. 1527–1536.

List of Figures

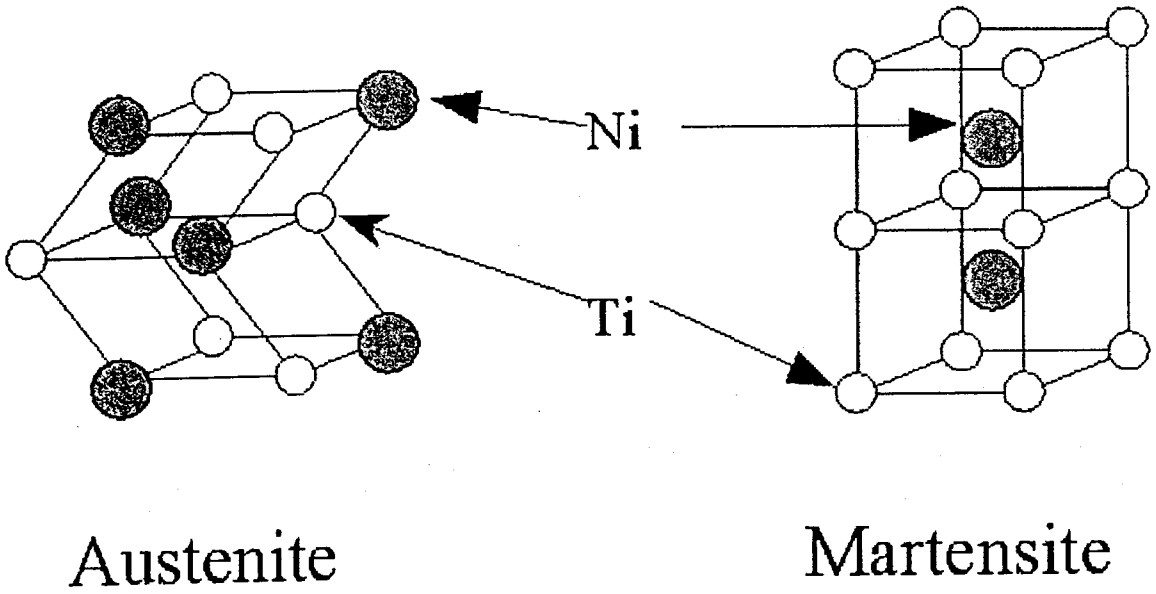

Figure 1: Martensite and Austenite crystal

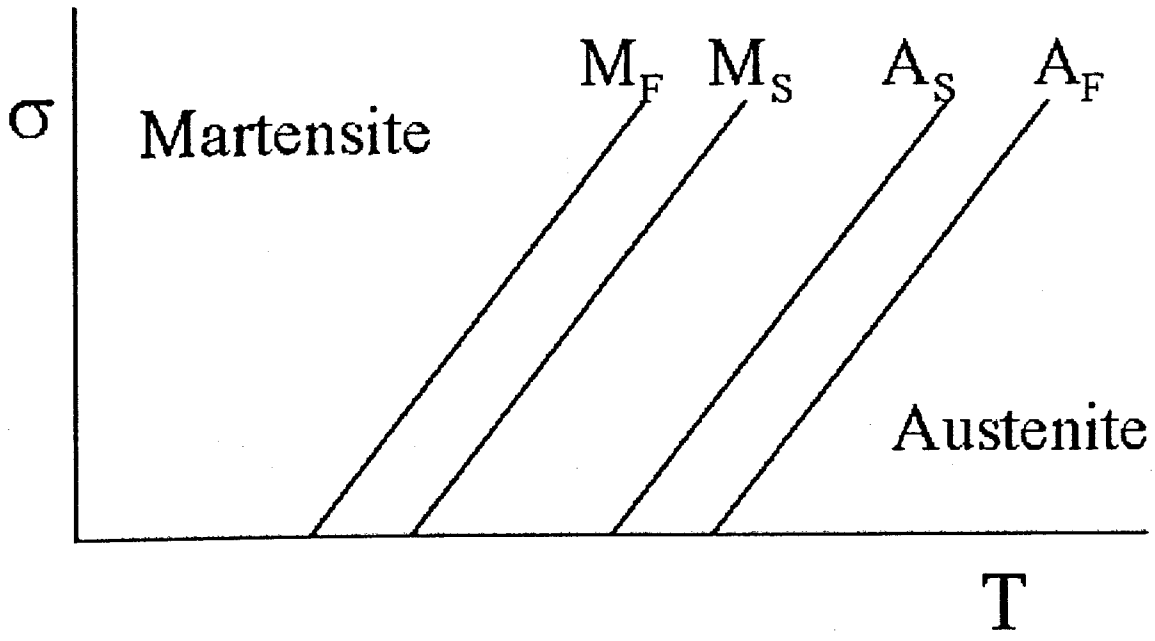

Figure 2:Typical stress temperature phase diagram for NiTi(SMA)

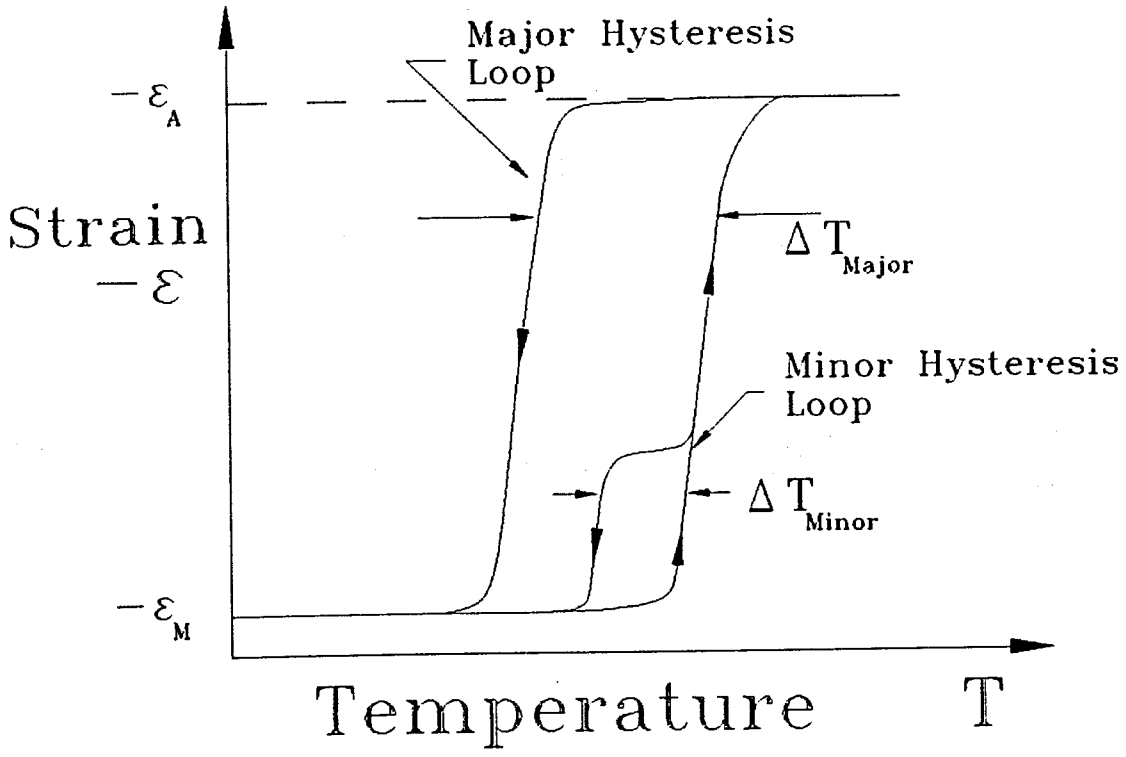

Figure 3:Strain-temperature SMA transformation diagram.

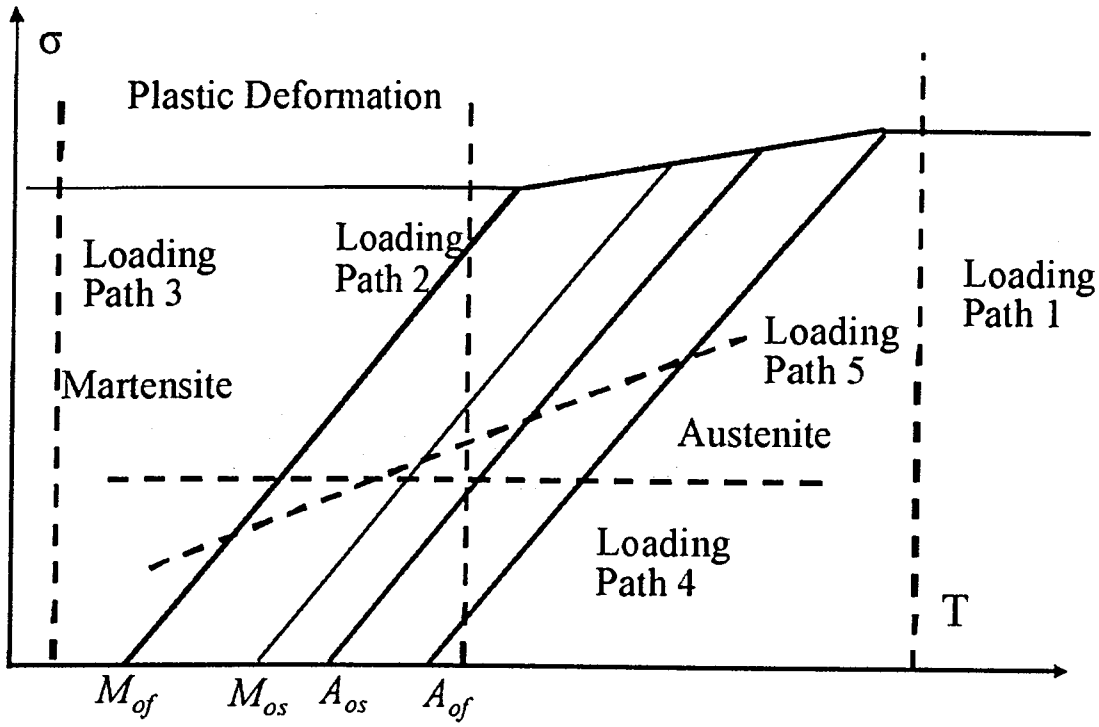

Figure 4:Representation of fatigue loading paths in stress vs. temperature space.

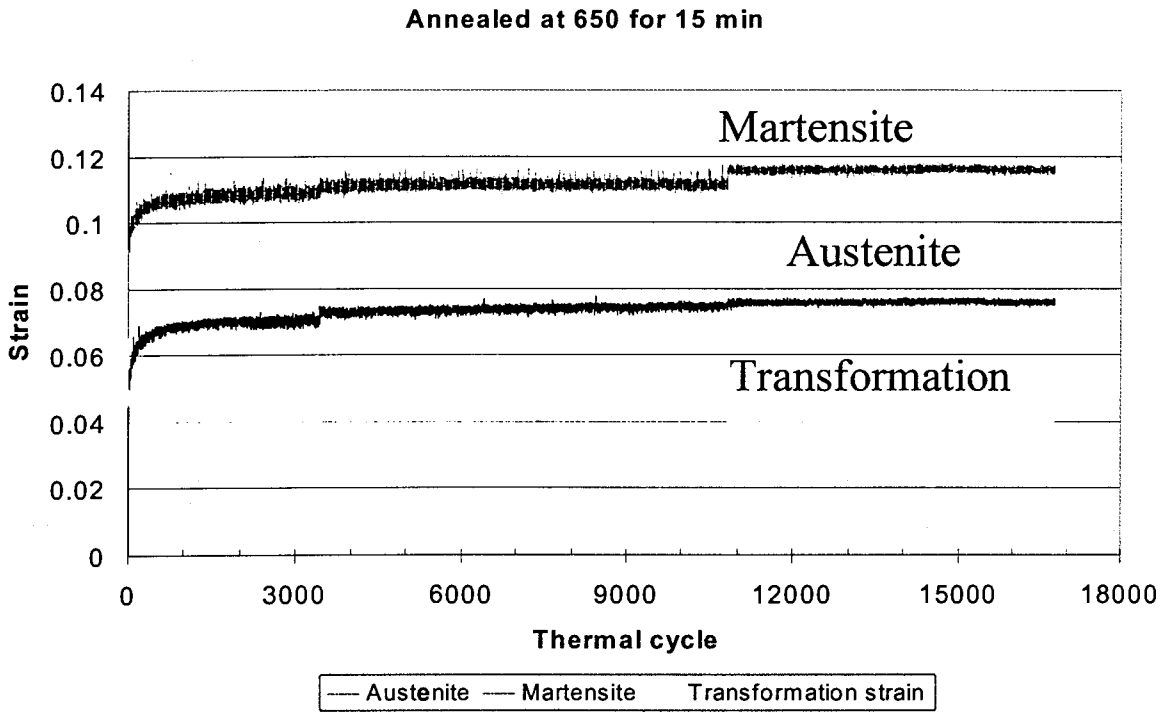

Figure 5: A typical curve of thermomechanical fatigue of NiTiCu annealed at 650°C for 15 min.

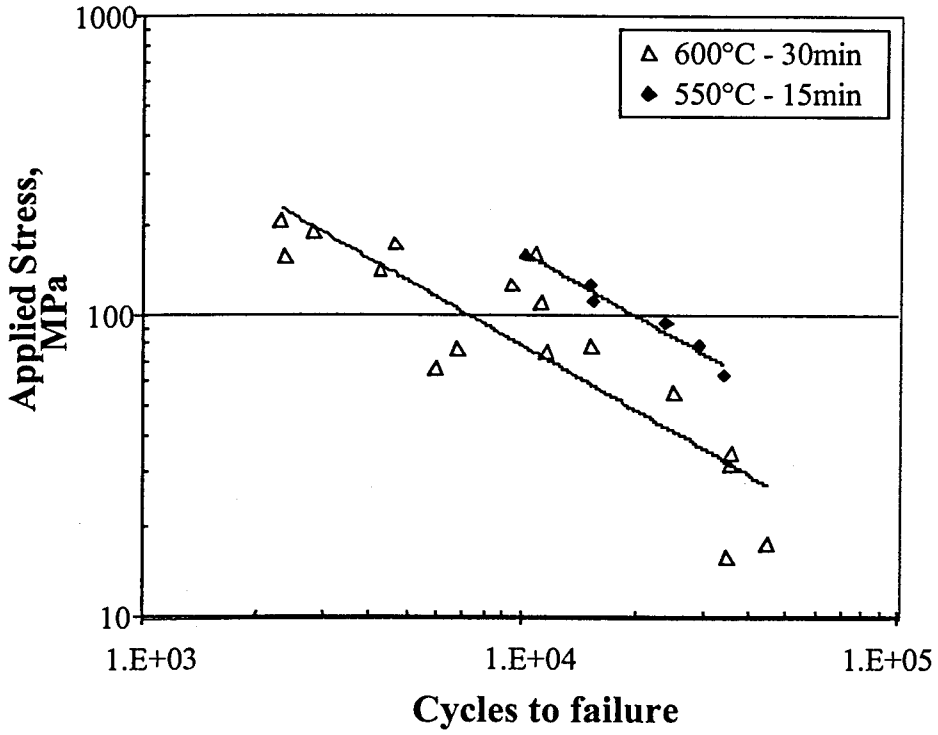

Figure 6: Applied stress vs. thermal cycles to failure for NiTiCu SMA for a complete transformation

$$\lambda^{a} = \frac{\varepsilon^{T}_{\max} - \varepsilon^{T}_{\min}}{2H^{T}_{\max}} = \frac{\lambda^{\max} - \lambda^{\min}}{2} \qquad \lambda^{0} = \frac{\varepsilon^{T}_{\max} + \varepsilon^{T}_{\min}}{2H^{T}_{\max}} = \frac{\lambda^{\max} + \lambda^{\min}}{2}$$

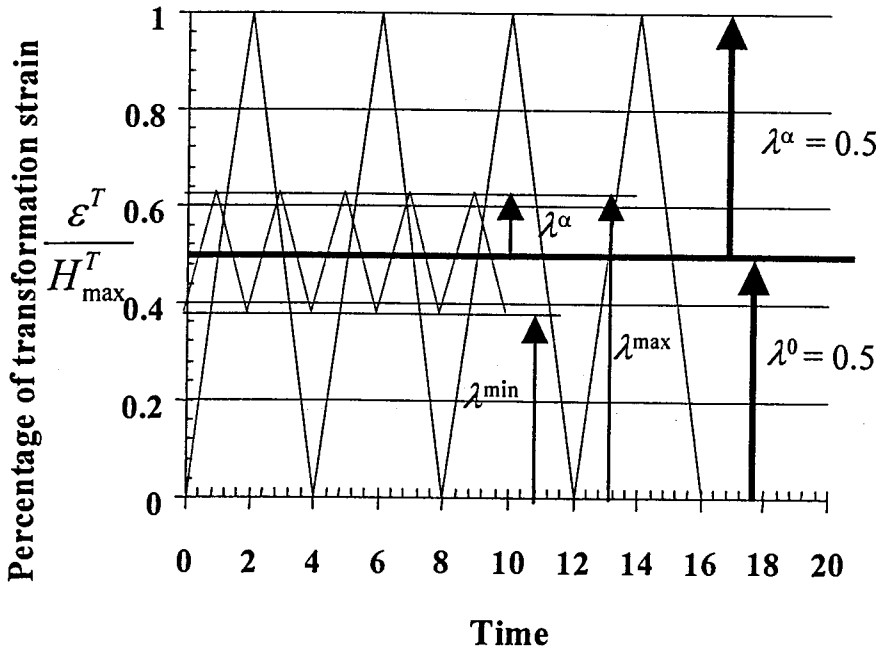

Figure 7:Schematic of partial transformation loops showing physical meaning of the mean percentage of transformation strain λ^0 and the amplitude of transformation strain percentage λ^a.

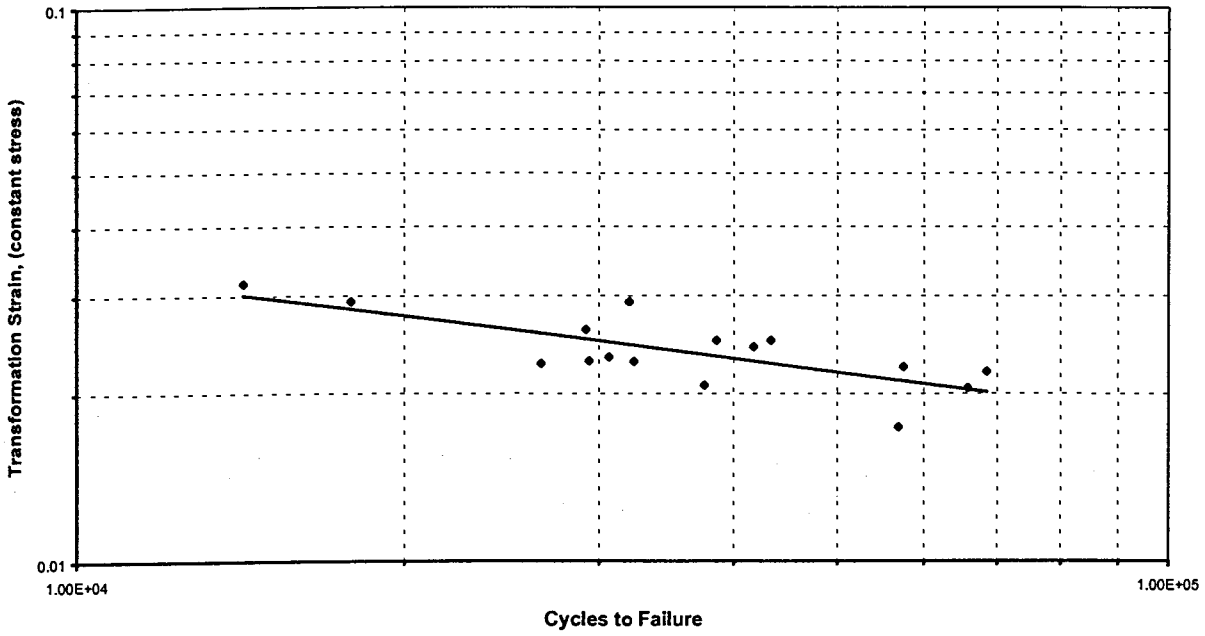

Figure 8: The effect of transformation strain on the thermal transformation fatigue life for minor hysteresis loops.

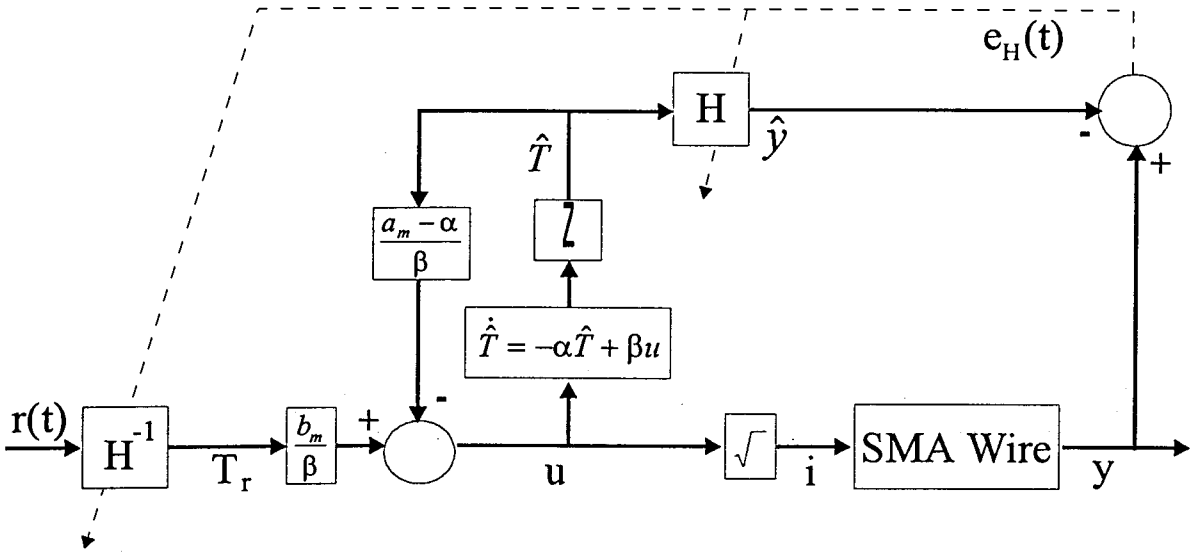

Figure 9: SMA control scheme.

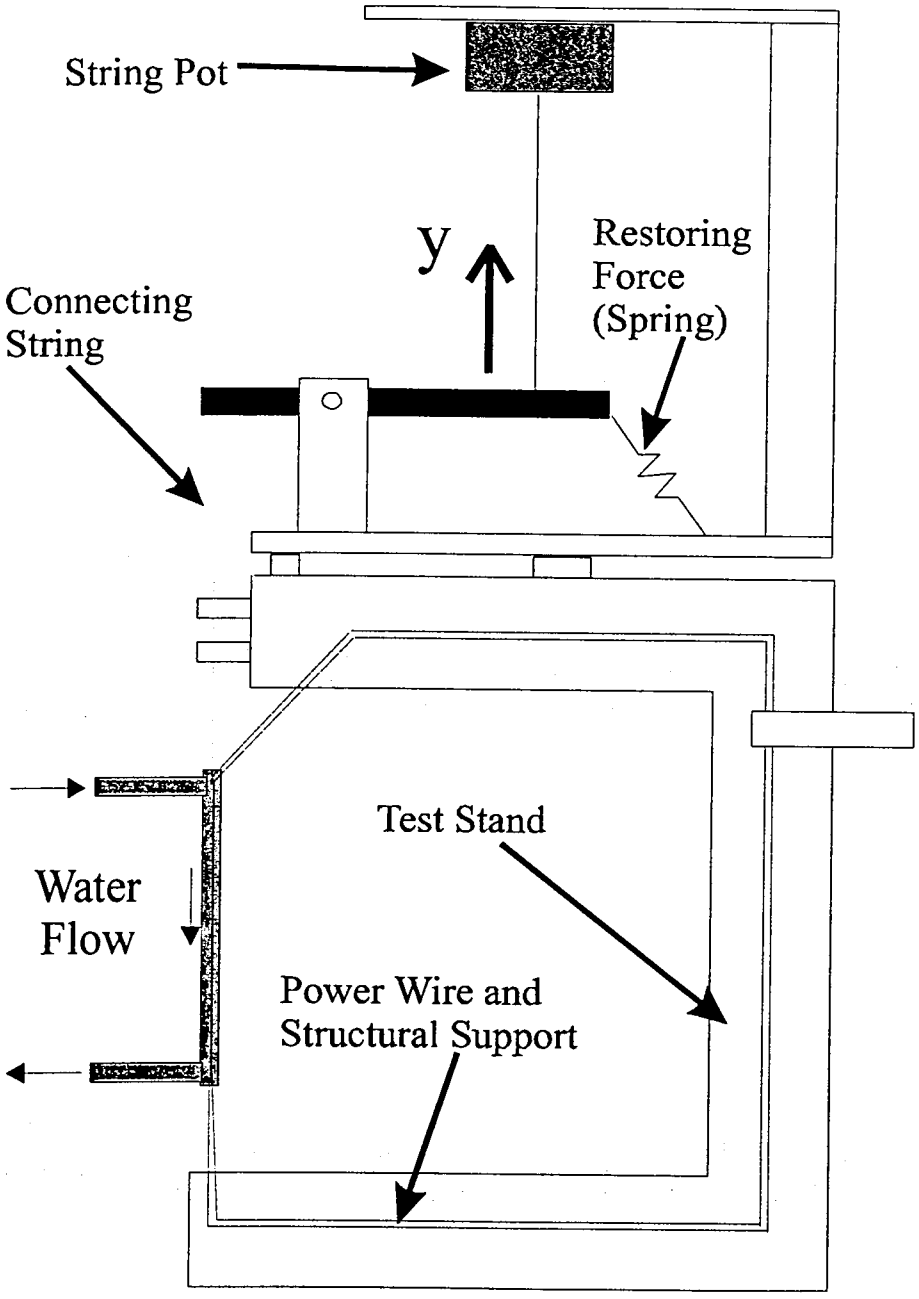

Figure 10: SMA control test stand.

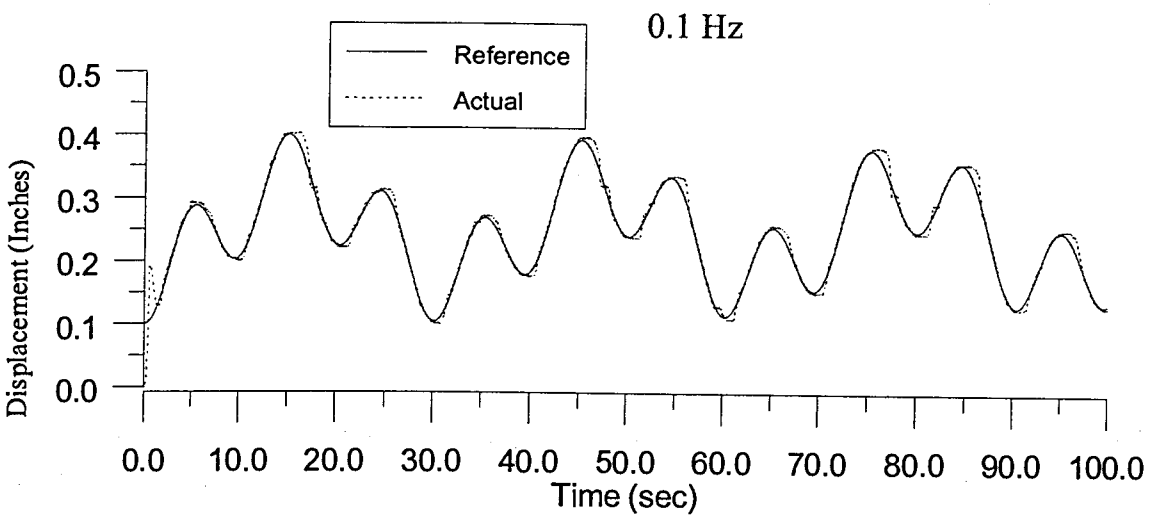

Figure 11:Forced air convection cooling

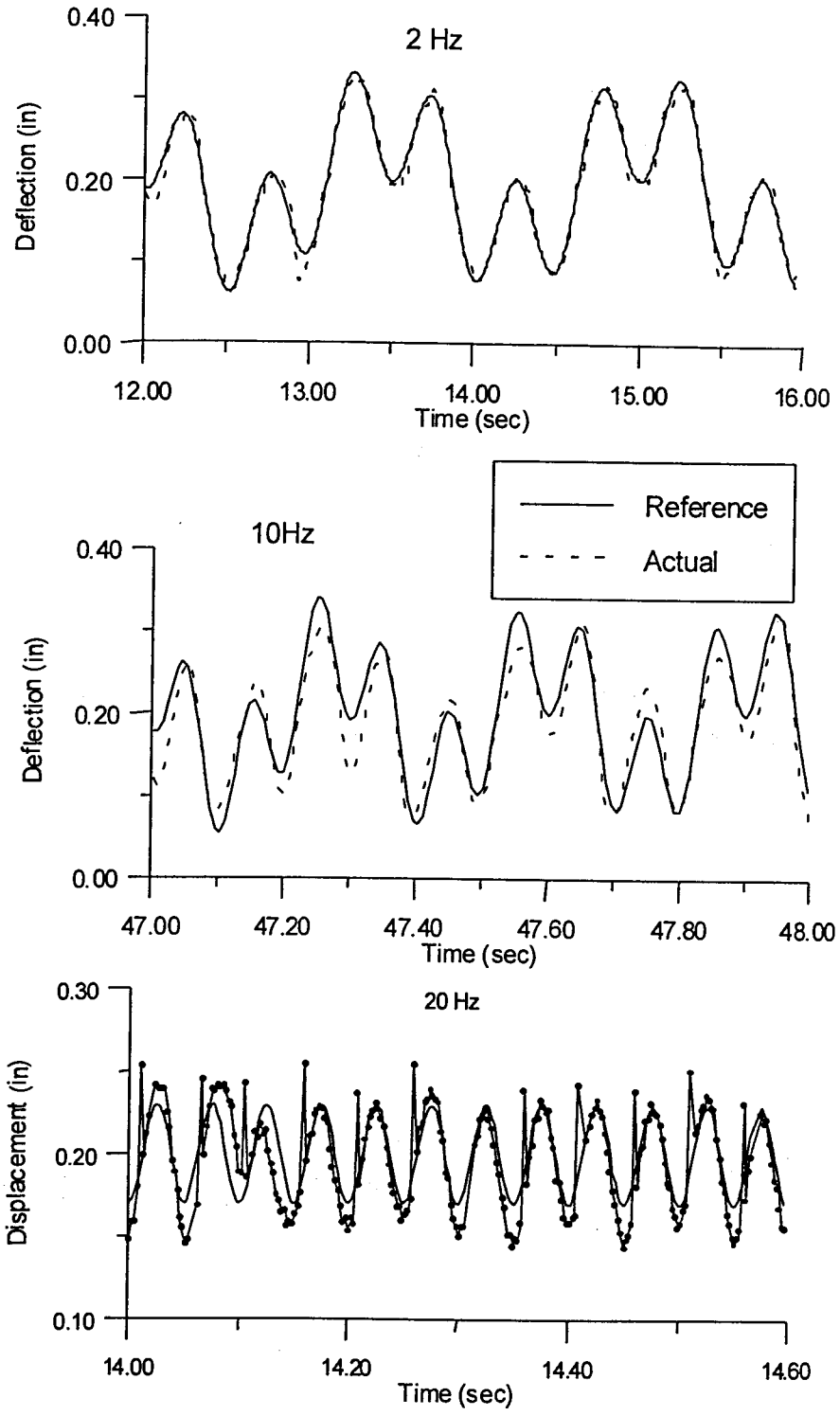

Figure 12:SMA Actuator control using an adaptive hysteresis model with active cooling.

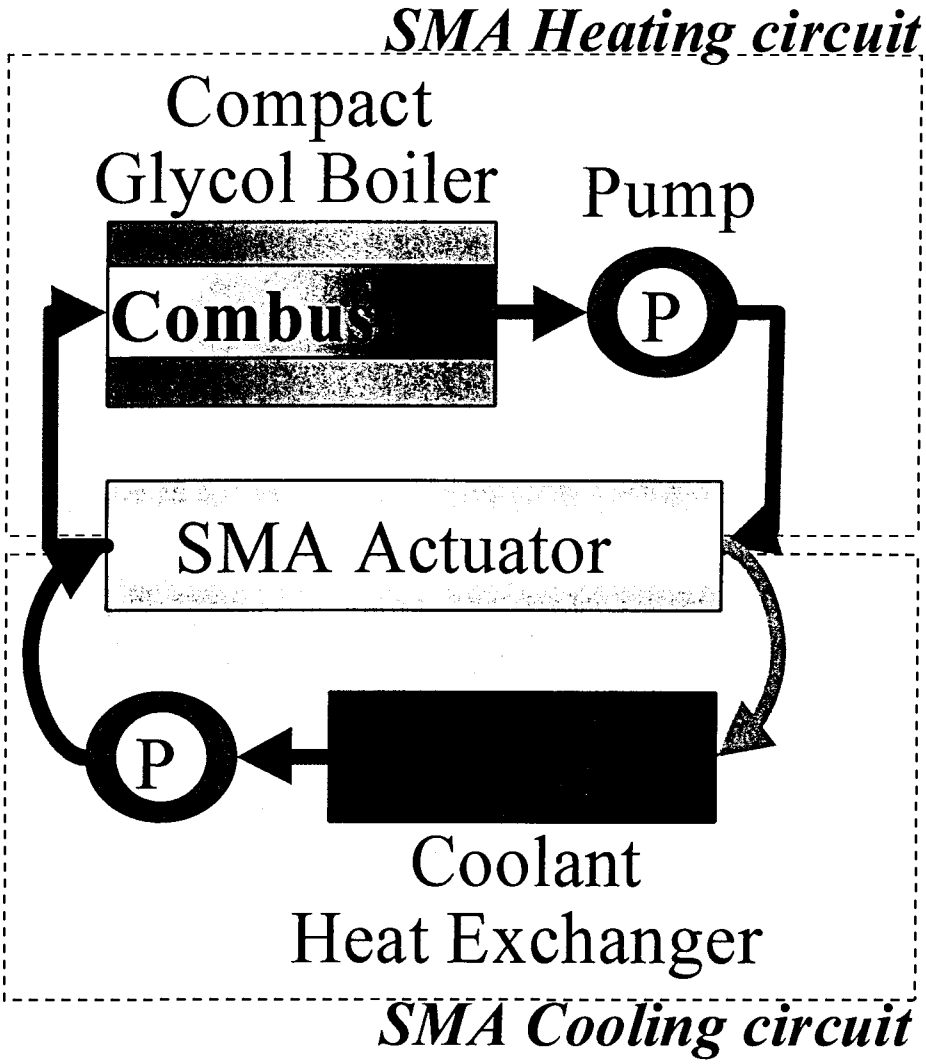

Figure 13:Compact actuator system.

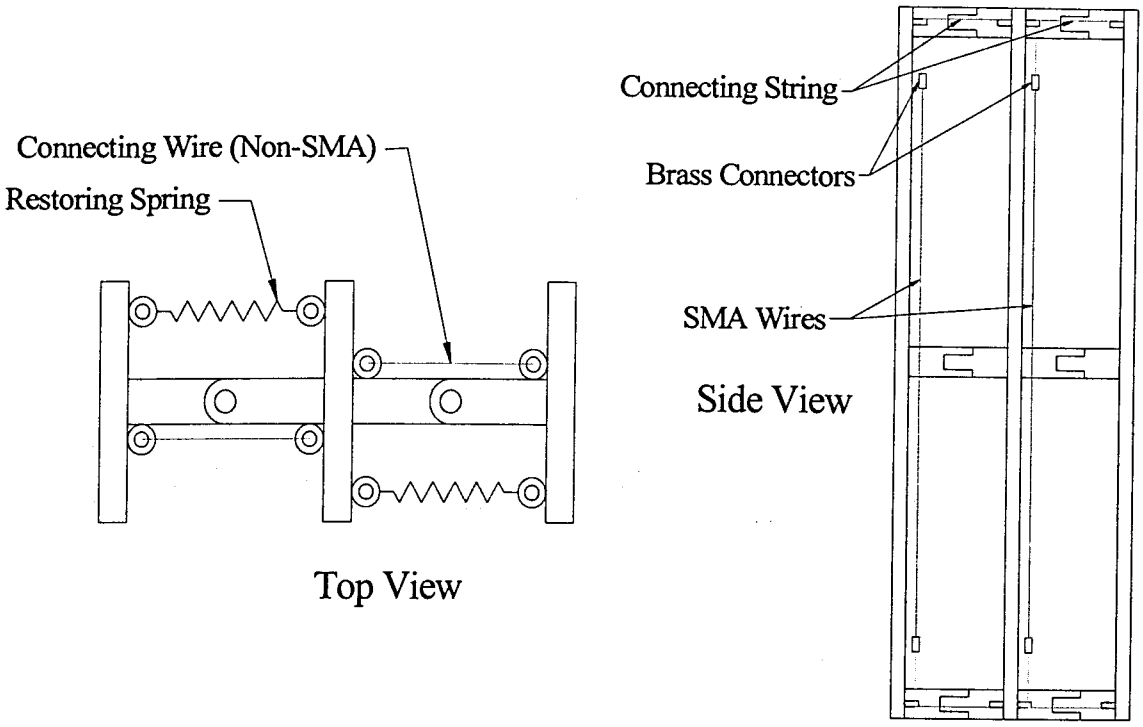

Figure 14: Schematic of SMA muscles on biomimetic hydrofoil.

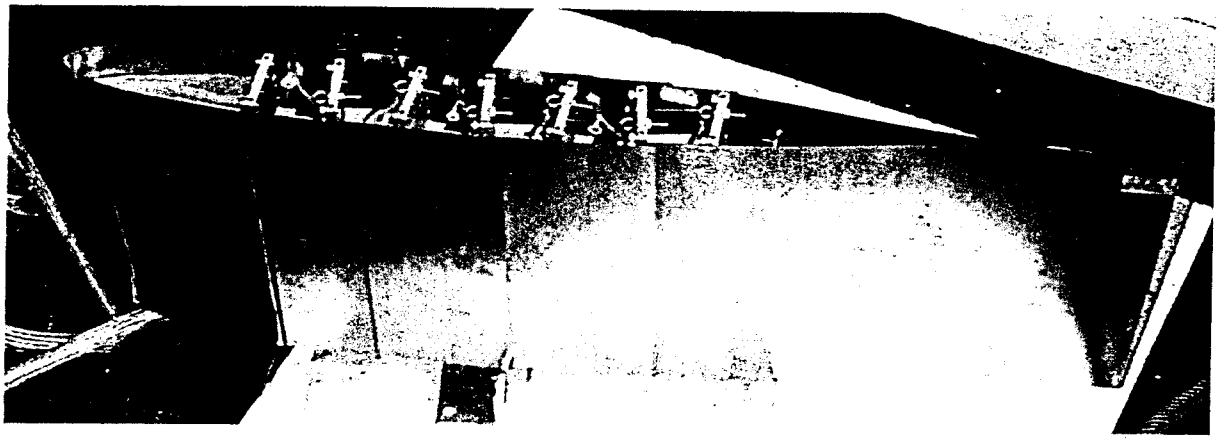

Figure 15: Assembled biomimetic hydrofoil.

Figure 16: Photograph of a tail position during an actuation cycle in the water tunnel.